#### **TOPICAL REVIEW**

## Imaging of soft materials using *in situ* liquid-cell transmission electron microscopy

To cite this article: Kun He et al 2019 J. Phys.: Condens. Matter 31 103001

View the article online for updates and enhancements.

#### Recent citations

- <u>TEM Studies on Antibacterial Mechanisms</u> of Black Phosphorous Nanosheets Abhijit H Phakatkar *et al*
- In-Situ Visualization of Ferritin Biomineralization via Graphene Liquid Cell-Transmission Electron Microscopy Surya Narayanan et al
- Transmission electron microscopy of the iron oxide core in ferritin proteins: current status and future directions
  Surya Narayanan et al



## IOP ebooks™

Bringing together innovative digital publishing with leading authors from the global scientific community.

Start exploring the collection-download the first chapter of every title for free.

#### **Topical Review**

# Imaging of soft materials using in situ liquid-cell transmission electron microscopy

Kun He<sup>1</sup>, Tolou Shokuhfar<sup>2</sup> and Reza Shahbazian-Yassar<sup>1,3</sup>

- Department of Mechanical and Industrial Engineering, University of Illinois at Chicago, Chicago, IL 60607, United States of America
- <sup>2</sup> Department of Bioengineering, University of Illinois at Chicago, Chicago, IL 60607, United States of America

E-mail: rsyassar@uic.edu

Received 20 January 2018, revised 28 October 2018 Accepted for publication 4 December 2018 Published 18 January 2019



#### **Abstract**

This review summarizes the breakthroughs in the field of soft material characterization by *in situ* liquid-cell transmission electron microscopy (TEM). The focus of this review is mostly on soft biological species such as cells, bacteria, viruses, proteins and polymers. The comparison between the two main liquid-cell systems (silicon nitride membranes liquid cell and graphene liquid cell) is also discussed in terms of their spatial resolution and imaging/analytical capabilities. We have showcased how liquid-cell TEM can reveal the structural details of whole cells, enable the chemical probing of proteins, detect the structural conformation of viruses, and monitor the dynamics of polymerization. In addition, the challenges faced by decoupling electron beam effect on beam-sensitive soft materials are discussed. At the end, future perspectives of *in situ* liquid-cell TEM studies of soft materials are outlined.

Keywords: *in situ* TEM, soft materials, high resolution imaging (Some figures may appear in colour only in the online journal)

#### 1. Introduction and background

A significant challenge in microscopy is to image or probe soft materials such as biological cells, bacteria, viruses, biomolecules, and proteins at sub-nanoscale placed in hydrated environment. Transmission electron microscopy (TEM) has emerged as an extremely powerful tool to image the structure of soft materials at unprecedented resolutions. However, volumetric shrinkage, electrostatic charging, and structural degradation of soft materials contribute to the radiation of incident electron beam in a high vacuum environment. Therefore, to overcome these drawbacks, the TEM studies of such materials have been employed under cryo or substrate-embedded conditions (microtoming procedure) and relatively low voltage

TEM imaging [1–6]. Unfortunately, these techniques are restricted by several shortcomings: (1) soft materials may be deformed by the stain (sometimes severely) [7, 8]; (2) similarity in densities of soft materials and vitrified water contribute to limited Z contrast imaging and low signal to noise ratio, accordingly, majority of cryo-samples are negatively stained to increase contrast, in spite of plastic deformation caused by negative stain [9, 10]; (3) in cryo-imaging procedure, the specimens must be maintained at less than  $-135\,^{\circ}\text{C}$  requiring expensive cryo-TEM facility and specimen preparation instruments; and (4) the vitrification process and sample preparation for microtoming requires extensive trial and errors to achieve impeccable results [7, 10, 11].

The recent development of liquid-cell TEM technique provides unprecedented capabilities to image and analyze samples in a liquid environment, with both high spatial and high

<sup>&</sup>lt;sup>3</sup> Author to whom any correspondence should be addressed.

temporal resolutions. This technique allows to observe the dynamics of materials in liquid solutions at sub-nanometer resolution. For instance, the nucleation and growth of nanoparticles in liquid solutions [12–16], electrochemical behavior of nanomaterials [17-22], have successfully been conducted using in situ liquid-cell TEM technique. Yet, in situ liquidcell TEM application in biological field is relatively limited, although it has been used extensively for fixation in epoxies materials science. Thus, the major challenge is to understand the biological cell function or detailed structure of bacteria or virus at their native liquid environment which could be difficult due to their low atomic number following by relatively weak TEM contrast [23]. In spite of all these challenges, there has been a growing number of biological structures and soft materials using liquid-cell TEM-related studies which have resulted in significant progress in the area of biology and the science of soft materials. Therefore, we discuss, in this review, different approaches which researchers have applied to use liquid TEM in order to evaluate soft materials. Accordingly, researches have mostly focused on whole cell imaging in liquid media, detection of detailed structure of viruses, and chemical signature of hydrated proteins. Consequently, we anticipate that this review brings more attention to the applications of liquid-cell TEM technique to investigate soft materials. At the end, the radiolysis and beam effect on the soft materials are discussed to provide a clear picture in terms of understanding how the electron beam affects the soft materials and how to prevent or take advantage of this effect for future research in this field.

The setup of a liquid-cell TEM experiment can be divided into flow and static modes based on the way by which the liquid is introduced into the TEM chamber. At the early stage of liquid cell development in 2003, a homemade static liquid cell chips using two silicon chips was sealed by epoxy [24]. Moreover, the electron transparency was guaranteed by the use of silicon nitride membranes embedded in the two silicon chips which had minimum scattering effect on the incident electron beam (figures 1(a) and (b)). The thickness of the liquid confined within the two windows was about 100 nm, where the spatial resolution for the liquid-cell TEM could reach 5 nm [24]. Later on, several commercial liquid holders were developed with capability of liquid flow-mode, such as Protochips [14, 22, 25, 26], Hummingbird [27–30], and DENS Solutions [31]. The liquid flow is enabled by the inlet and outlet channels connected to the tip area of the TEM holder, which are used as channels to guide the liquid flow (figure 1(c)). The flow rate for the liquid holder should be lower than 300  $\mu$ l h<sup>-1</sup>. If the flow rate is higher than this value, the SiN membranes are easy to be broken. Normally, at nanoscale the moving of particles could be traced. For the biological cell and bacteria, the size of the sample is large, and the sample is cultured attached to the membrane, so there is no restrict for the flow at this circumstance. Considering the thickness reduction of the silicon nitride membrane down to 20-50 nm, the spatial resolution of liquid-cell imaging using the silicon chips has reached sub-nanometer scale [32].

In addition to the Si chip-based liquid-cell design, another novel liquid-cell design has been developed based on graphene membranes [33, 34]. Two-dimensional (2D) graphene has been regarded as a good candidate to confine liquid in TEM vacuum chamber due to its mechanical stability [35], non-permeability to water [36], good conductivity [37], and good electron transparency [38]. The thickness of monolayer or multilayer graphene (1–10 nm) is extremely thin compared to silicon nitride membranes used for flow liquidcell [39, 40]. In addition, the atomic number of carbon atom (Z = 6) is lower than silicon (Z = 14) atom and nitride atom (Z=7), which significantly reduces the electron scattering by this cell design. As a result, the resolution of graphene liquid cell (GLC) imaging is improved significantly to 0.1 nm (figure 1(d)) [41]. The strong van der Waals forces between two graphene sheets limit the size of the GLC pockets to be less than 200 nm [41]. The pressure can reach a high level because of the van der Waals forces. This high pressure may cause some side effect on the sampled encapsulated. This can be a disadvantage when required to study the behavior of liquids under less confinements or more liquid flow. Taking the advantage of both Si chip design and GLC design, a new method was developed as shown in figure 1(e), where graphene was used to enclose the samples and liquid cultivated on silicon microchip with a silicon nitride membrane. This method allowed the biological cells to be cultured and labeled as usual.

### 2. Research on soft materials using *in situ* liquid TEM

Recent developments in advanced nanoscale characterization techniques have increased the quantity and quality of *in situ* liquid-cell TEM studies of organic matter specifically biological samples. Based on the characteristics of these low contrast biological samples, heavy metals such as gold nanoparticles or quantum dots can be used to label certain protein or ligand for increasing the contrast. Therefore, by detecting the gold nanoparticles or quantum dots, intracellular or extracellular vesicles can be detected and cellular activities can be monitored by liquid-cell TEM. Moreover, the studies focused on non-biological materials such as polymers, hydrogels, and liposomes will be discussed in this review.

Main concern of this technique is the effect of electron beam on soft materials as it is not neglectable comparing to hard materials. However, the effective control of the electron beam could alter the chemistry and pH of the environment resulting in discovery of new phenomenon and mechanisms. In general, liquid (S)TEM provides a unique approach to study the structures of biological samples under native and hydrated conditions. This has been significantly improved in terms of the spatial resolution and imaging speed. Table 1 summarizes the previous in situ liquid-cell TEM observations of soft materials. In fact, one big challenge of liquid cell TEM imaging is the resolution decrease caused by the addition of the membranes used to encapsulate the liquid solution. In general, the thicker the membranes are, the lower the resolution will be. This is also true for the amount of liquid solution surrounding the object, namely more liquid solution will reduce the resolution as well. The resolution of GLC is higher than

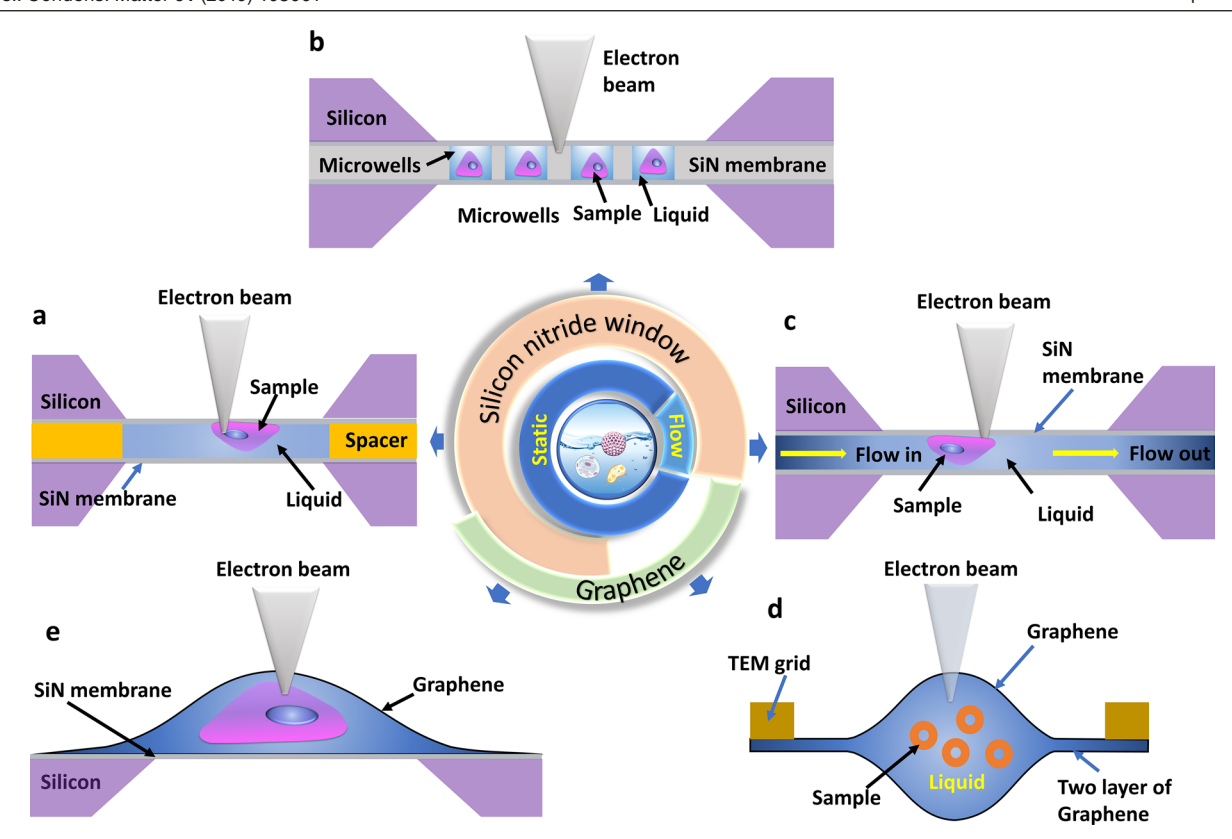


**Figure 1.** Schematic of various fluidic cell designs for *in situ* liquid-cell TEM studies. The center circle describes the classifications of liquid-cell techniques based on the static or liquid flow modes. The most successful liquid-cell techniques in TEM are based on either silicon nitride membranes or graphene sheets: (a) microfluidics with built-in silicon nitride membranes for static mode imaging; (b) multi-window silicon nitride membranes; (c) liquid-flow microfluidic silicon devices with silicon nitride membranes; (d) graphene liquid cell; and (e) graphene/silicon nitride cell.

the silicon nitride membrane liquid cell. As clearly seen, the spatial image resolution could reach 1 nm during GLC imaging, while this is far from ideal in the silicon nitride liquid-cells. Generally, variety of biological structures such as cells, bacteria, and viruses, as well as soft materials such as polymer molecules have been imaged via liquid-cell TEM technique.

#### 2.1. Biological cells, bacteria, and viruses

The first in situ liquid-cell TEM study of whole biological cells was reported by De Jonge et al in 2009 [42]. This came after successful utilization of microfluidic liquid-cell TEM to image nanoparticles in 2003 [24]. The reason for this time gap was the challenges related to the culture of biological cells on silicon nitride membranes and the technical difficulties for keeping biological cells hydrated and intact during imaging under electron beam. Klein et al [60] compared the visibility of gold nanoparticle-labeled cells in their dry and wet conditions. They claimed that the edges of biological cells could be imaged at dry condition, however, in liquid media, only the gold nanoparticles could be observed [60]. De Jonge [42] and his co-workers used electron transparent silicon nitride membranes to visualize the fixed fibroblast cells by STEM. In their procedure, the buffer solution was flowed between the two silicon nitride chips which were used to keep cells hydrated and also ensure a complete filling of sample compartment with liquid. Accordingly, the thickness of the biological cell reached around  $7 \pm 1 \mu m$ . Furthermore, the spacer between SiN chips was 10  $\mu$ m which could be considered sufficiently thick for the accommodating the biological cells. However, such thick liquid dramatically lowered the resolution of the image. Therefore, single gold-tagged epidermal growth factor (EGF) molecules bound to cellular EGF receptors was used to increase the resolution. By using this label, the spatial resolution could reach 4nm, and, the gold nanoparticles could be imaged, nevertheless, the intra cellular structure of the biological cell still remained obscure during imaging. The similar method was also applied to test the visibility of gold nanoparticle-labeled epidermal growth factor receptor for COS7 cells and E. coli bacterium at static mode by sealed silicon nitride chips [23]. The contour of bacterium was observed fuzzy under hydrated status using a homemade liquid-cell. At lower magnification, only some cluster of the gold nanoparticles were visible, while at higher magnification, the gold nanoparticles could be clearly detected [23]. The outline of the cell could be distinguished but it was somehow impossible to detect inside of label free cell in details as shown in figure 2(a). Later, a specially designed microwell chip (figure 1(b)), which was pretreated by protein for better cell attachment to the SiN window, was introduced [43]. This method raised the possibility of reporting the interactions of gold nanoparticle with glioblastoma stem cells (GSCs) (figure 2(b)), and helped to investigate the cytotoxicity of the gold nanoparticles to the GSCs at nanoscale. In fact, it was

**Table 1.** A summary of soft materials imaged by liquid-cell (S)TEM.

Ref.	Flow status	Specimen	Liquid solution	Specimen size	Liquid-cell type	Spatial resolution
[42]	Yes	Fibroblast cells	10% PBS buffer	10 nm gold nanoparticle labeled micrometer size cell	SiN window flow cell	4 nm
[23]	No	Mammalian cells (COS7)  Escherichia coli bacteria	10% PBS buffer	Gold labeled micrometer size bacteria/ gold labeled micrometer size cell	SiN window cell	3 nm
[43]	No	Glioblastoma stem cells	Buffer solution containing 20 mM HEPES (pH, 7.5), 150 mM NaCl, 20 mM CaCl <sub>2</sub> , 20 mM MgCl <sub>2</sub> ,	10–100 nm gold nanoparticles and micrometer size cell	SiN window microwell chip	_
[26]	No	Extracellular vesicles and artificial liposomes	Cell medium	<500 nm	SiN window cell	Sub 5 nm
[33]	No	Breast cancer cells	Desalinized water	10 nm gold particles labeled micrometer size cell	Graphene liquid enclosure on silicon nitride chip	2 nm
[44]	No	Fibroblast cells/lung cancer cells	DMEM, supplemented with 10% FBS	12 nm Au particles labeled micrometer cell	Environmental TEM/	3 nm
[45]	Yes	Cupriavidus metallidurans	50 mM AuCl medium	$1$ – $2~\mu m$	SiN window cell	NA
[36]	No	bacterium	Deionized water	$2.73 \pm 0.96 \ \mu\text{m}^2$	Graphene	0.4 um
[46]	Yes	Magnetotactic bacteria	Standard media	Micrometer	SiN window cell	_
[47]	No	Magnetospirillum magneticum	Flask standard medium	$13~\mu\mathrm{m}$ in length and $400600\mathrm{nm}$ in diameter	SiN window cell	NA
[48]	Yes	E. coli and P1 bacteriophages	Potassium morpholinopropane sulfonate (MOPS)	Micrometer	SiN window flow cell	5 nm
[49]	Yes	E. coli	Potassium morpholinopropane sulfonate (MOPS)	Micrometer	SiN window flow cell	5 nm
[50]	Yes	PdAu decorated Geobacter sulfurreducens cell	Au(III)Cl <sub>3</sub> and Na <sub>2</sub> Pd(II)Cl <sub>4</sub> in H <sub>2</sub> O	Several hundred nanometer	SiN window cell	nanometer
[51]	Yes	Rotavirus (RV) double layered particles (DLPs)	100 mM tris-HCl, 6 mM MgAc, 4 mM DTT, 2 mM each of ATP, GTP, CTP, UTP, and 1 $\mu$ l RNasin	~50 nm	SiN window cell	2.8 nm
[52]	Yes	Ferritin and nanolipoprotein discs	10 mM tris, 100 mM NaCl	12 nm	SiN window cell	2 nm
[30]	Yes	Protein Mms6	Ferric chloride solution	25–150 nm	SiN window cell	
[53]	Yes	Lysozyme	Lysozyme solution and NaCl solution	170 nm	SiN window cell	
[54]	No	Ferritin	Water	12 nm	Graphene	0.99 nm
[55]	No	PEGylated Interferon $\alpha_{2a}$	HEPES buffer		SiN window cell	
[56]	No	Micellar nanoparticles consisting of a Pt(II)-labeled core	Dry DMF	~90 nm	SiN window cell	
[57]	No	Double strand DNA	NaCl solution and poly(ethylene glycol) methyl ether thiol (MPEG)	5 nm gold	Graphene	
[58]	No	Micellar nanoparticles	DMF	~20 nm	SiN window cell	Nm
[59]	No	Polystyrene sulfonate and poly (ethylene oxide)	0.2 m NaCl	5–60 nm	Graphene	Nm

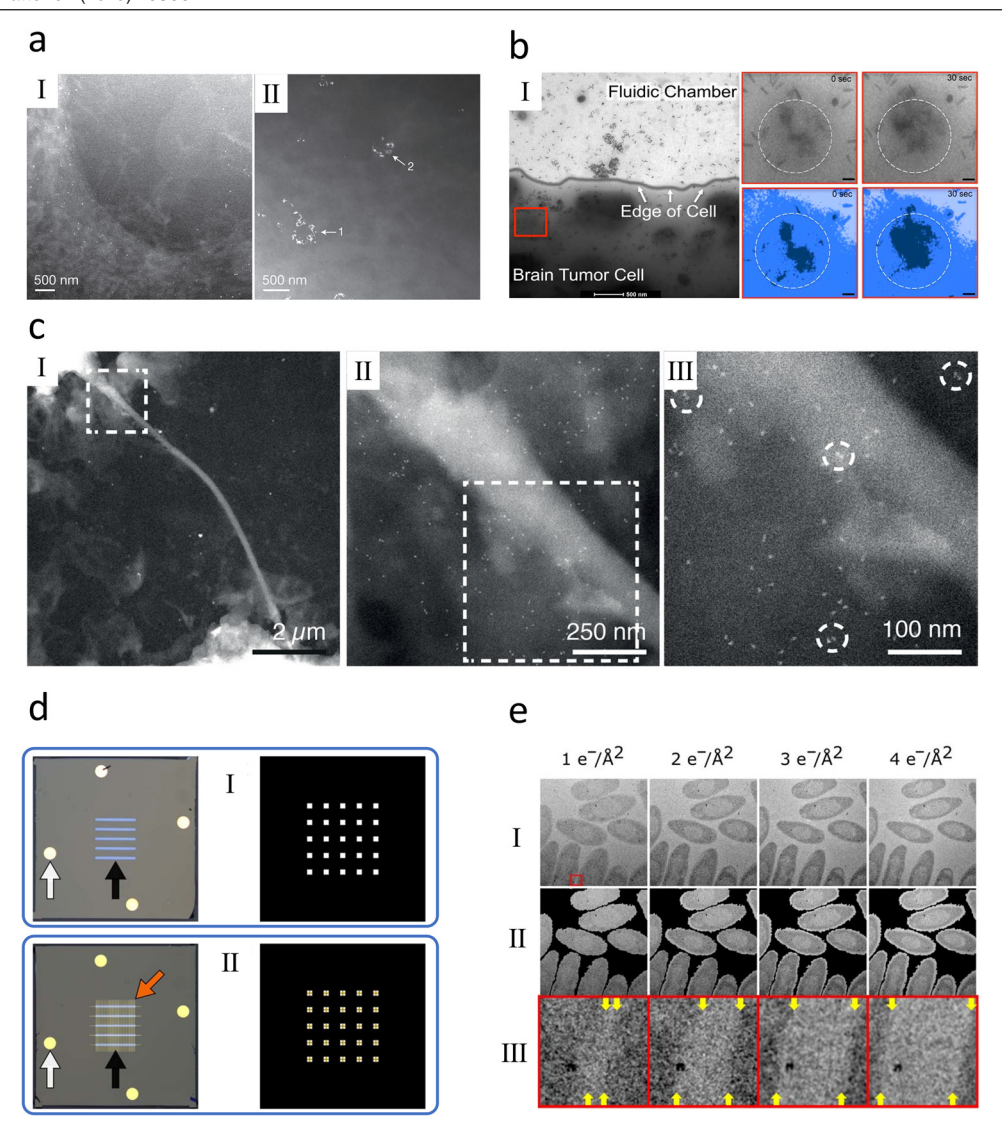


Figure 2. Liquid-cell TEM imaging of biological cells. (a) Liquid-cell STEM images of COS7 fibroblast cells labeled by EGF-Au. Reproduced with permission from [42]. (b) Gold nanorods are shown to be mobile within glioblastoma (brain tumor) stem cells. Reprinted with permission from [43]. Copyright 2015 American Chemical Society. (c) STEM images of quantum dots (QDs)-labled ErbB2 proteins in hydrated SKBR3 breast cancer cells in graphene-covered hydrated cells. Reprinted with permission from [33]. Copyright 2017 American Chemical Society. (d) and (e) The multi-window device for liquid-cell TEM and the effect of cumulative electron flux on biological cells (*C. metallidurans*) From [45]. Reprinted with permission from AAAS.

the first time to visualize the nanoparticle interactions with GSCs in real time. In a separate work, the dynamics of extracellular vesicles (EVs) was investigated using silicon nitride chip-sandwiched EVs. For this study, the cells were cultured by classical methods and then drop casted on the chip. The whole TEM experiments were done in low-magnification mode before and after the observation of EVs. In following, the flow mode of the liquid cells was used to minimize the bubble formation. It was also demonstrated that the electron beam could induce the formation of gold nanoparticles around the liposomes and EVs which have phospholipids in common. This in situ gold staining method with sub 5 nm resolution, and an efficient generic method was employed to observe the morphological or topological details of biological specimens by liquid-cell TEM [26]. Studying the extracellular vesicles by this liquid-cell method provides dynamic information of the vesicles interaction with cell and also inspires intracellular studies using similar devices [61]. The silicon nitride-based liquid-cells enables 4nm resolution using gold nanoparticles. Nevertheless, further resolution improvement have been facing challenges in this designed method since the spacers have to be large enough to fully encapsulate biological cells. In order to improve the resolution, De Jongs group developed a new method to fabricate liquid-cells utilizing graphene to seal the enclosures (figure 1(e)). Accordingly, they were able to use quantum dots to label the membrane protein (ErbB2) in whole cell and observe the distribution of the labeled protein by TEM with 2nm resolution (figure 2(c)). The heterogeneity of protein stoichiometry at single-molecule level was quantified in various cellular regions of whole cells, and they concluded that activated ErbB2 growth factor receptors prefer the connecting ends of tunneling nanotubes [33]. One important progress in this method is the elimination of any spacer between the fluidic chips that typically reduces

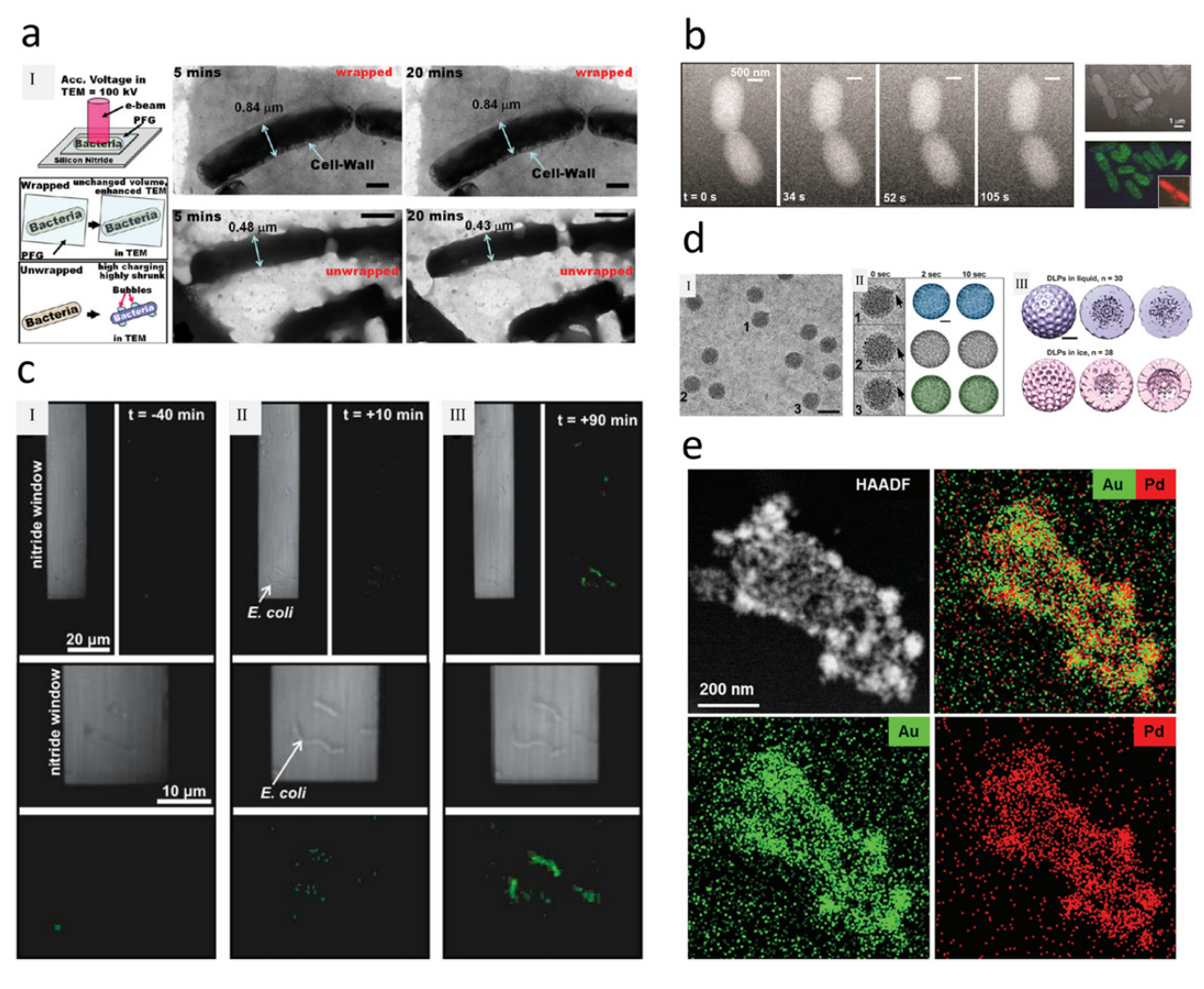
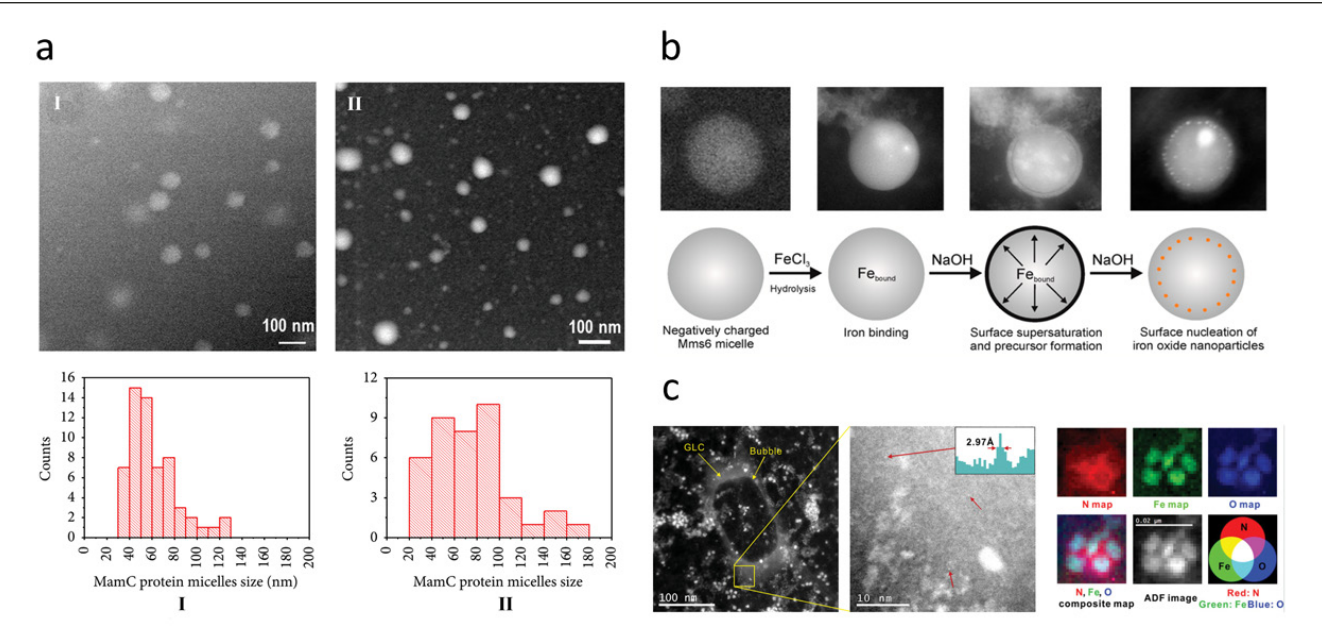


Figure 3. Liquid-cell TEM imaging of hydrated bacteria and viruses. (a) The GLC observation of bacteria (Bacillus subtilis) showed that the graphene wrapped bacteria did not shrink. Reprinted with permission from [36]. Copyright 2011 American Chemical Society. (b) The STEM snapshots of *E. coli* taken at different time intervals showing binary fission in *E. coli*, despite the stain and beam exposure. The live/dead assay of the same *E. coli* microcolony where green fluorescence indicates a live cell, while red fluorescence indicates a compromised membrane. Reprinted with permission from [48]. Copyright 2016 American Chemical Society. (c) Transmission optical micrographs of *E. coli* bacteria are shown prior to electron-beam irradiation (left), and after 10 min (middle) and 90 min (right) and the corresponding fluorescence micrographs. Reprinted with permission from [49]. Copyright 2017 American Chemical Society. (d) Representative virus (purified rotavirus (RV) double layered particles) in liquid with viral mRNAs transcripts and the 3D structure. Reproduced from [51] with permission of The Royal Society of Chemisty. https://pubs.rsc.org/en/content/articlehtml/2015/cc/c5cc05744b. (e) The STEM image and EDS maps of a single hydrated bacterium (*Geobacter sulfurreducens*) [50] John Wiley & Sons. © 2016 WILEY-VCH Verlag GmbH & Co. KGaA, Weinheim.

the spatial resolution. The same group used this method to observe A549 cell in hydrated status [44]. It provided another way to investigate cells with different thickness without sacrificing resolution by thick liquid enclosure. However, in this method, the liquid permeated between graphene and silicon nitride membrane is much less compared to typical microfluidic cells consisted of two silicon nitride membranes and spacers. For better quality of observation, which required to be associated with enough liquid for maintaining cell status, Moser *et al* [45] developed a new design for SiN membranes where multiple wells were fabricated on the microfluidic chips (figure 2(d)). The similar devices named fluorescence microscopy and environmental scanning electron microscopy (ESEM) might be useful to better observe whole structure of

cells [62–65]. Therefore, by combining the light fluorescence microscopy and STEM, the distribution of cell and local structural details could be precisely studied. By using this device, the membrane protein labeled by quantum dots (QD) could be used to study the metastasis [63] and drug response [65] of cancer cells.

In regard to the difficulty in TEM imaging of the live whole cells, several recent studies focused on bacteria, which were thinner than whole cells, and limited liquid environment in the liquid cell might be probably sufficient to keep them alive. The first *in situ* liquid-cell TEM of hydrated bacteria work was reported in 2011 [36], where the bacteria were wrapped using protein (concanavalin-A) functionalized graphene (PFG). The PFG wrapped bacteria could be imaged with their



**Figure 4.** Liquid-cell TEM imaging of protein structures. (a) *In situ* images and size distribution of micelles of biomineralization in liquid: (I) MamC before incubation and (II) after incubation with iron chloride. Reproduced from [72]. CC BY 3.0. (b) nucleation of iron oxide in Mms6 protein revealed by SiN liquid-cell TEM. Reprinted with permission from [30]. Copyright 2014 American Chemical Society. (c) STEM-HAADF images of ferritin proteins in GLCs and the corresponding EELS map [54] John Wiley & Sons.© 2014 WILEY-VCH Verlag GmbH & Co. KGaA, Weinheim.

original and unaffected dimensions, as shown in figure 3(a). The unwrapped bacteria were damaged easily at its cell wall by electron beam and bubble formation. The main reason for this damage was attributed to the high vacuum condition in the TEM column ( $\sim 10^{-5}$  Torr) causing a huge pressure difference in and out of the cell. Graphene, on the other hand, significantly alleviate this pressure difference by its strongly repelling  $\pi$  clouds in the interstitial sites of lattice and the C–C flexibility keeping the integrity of the wrapped bacteria. Although the live/dead tests to the bacteria were carried out just before the wrapping, it would be hard to determine if the bacteria were alive after the electron beam exposure.

Another report focused on studying the viability of bacteria such as E. coli under the electron beam. In order to improve the resolution of the image, 0.1% uranyl acetate (UA) was applied since the live/death test turned out to show a E. coli viability higher than 90% at this concentration of UA [48]. Figure 3(b) shows that the E. coli bacteria reproduce by a binary fission process, which is the direct evidence of their live status. The electron dose based live/dead arrays proved that the viability can reach 50% at a cumulative dose of 20 e<sup>-</sup>/nm<sup>2</sup>/frame, which is lower than the median lethal dose at 300 kV. The dynamic infection process of the E. coli strain by P1 bacteriophage was captured with a 5 nm resolution [48]. This work is the first proof showing that the bacteria were live inside the liquid-cell TEM holder during imaging [48]. They also demonstrated that the E. coli could be survived under 90 min of the electron beam exposure in low electron dose imaging (figure 3(c)) [49]. Another test shows that the structure of E. coli could keep intact in aqueous under e-beam [66]. It shown that the magnetotactic bacteria could be imaged by TEM through a SiN liquid-cell, where the chain of the magnetosome nanoparticles inside the bacteria and the cell

membranes could be clearly seen. The correlative fluorescence images of the bacteria after liquid TEM test showed that almost 50% of the bacteria could perfectly maintain membrane after 1 h in flow cell, although they did not indicate whether this test was done under electron beam or not. The existence of water inside liquid-cell and the integrity of bacteria were confirmed by the off-axis electron holograms combined with liquid-cell [47]. On the other hand, the claimed living status of cells during TEM imaging has also been questioned because even in the presence of the minimal electron dose, TEM contrast is several orders of magnitude higher than the threshold lethal dose level of a live cell [67]. Experiments have demonstrated the notable differences between fluorescence signals and the volumes of the cells before and after electron beam irritation, indicating a drastic change in the living status of the targeted cells [67, 68]. It is also shown that the cell structure could be damaged during the fluorescence-based characterization, although the fluorescence imaging results may indicate a live status of the cells [67]. The yeast cells also showed some volume shrinkage, as an indication of a dead status, while the fluorescence image indicated the yeast cells were alive. What's more, the vacuole signature was also lost during the fluorescence imaging, which is a typical characteristic of dead yeast cell. The observed 'binary fission' might also be implausible information caused by the volume shrinkage of the bacteria instead of the real natural biological process. Therefore, the question proposed on the possibility of live cell imaging seems reasonable [67]. Recently, the electron beam has been identified to have a direct effect on the volume shrinkage of C. metallidurans bacteria, though the resolution of structural imaging was not high enough to tell the living status of the bacteria [45]. A recent work has supported the possibility of imaging

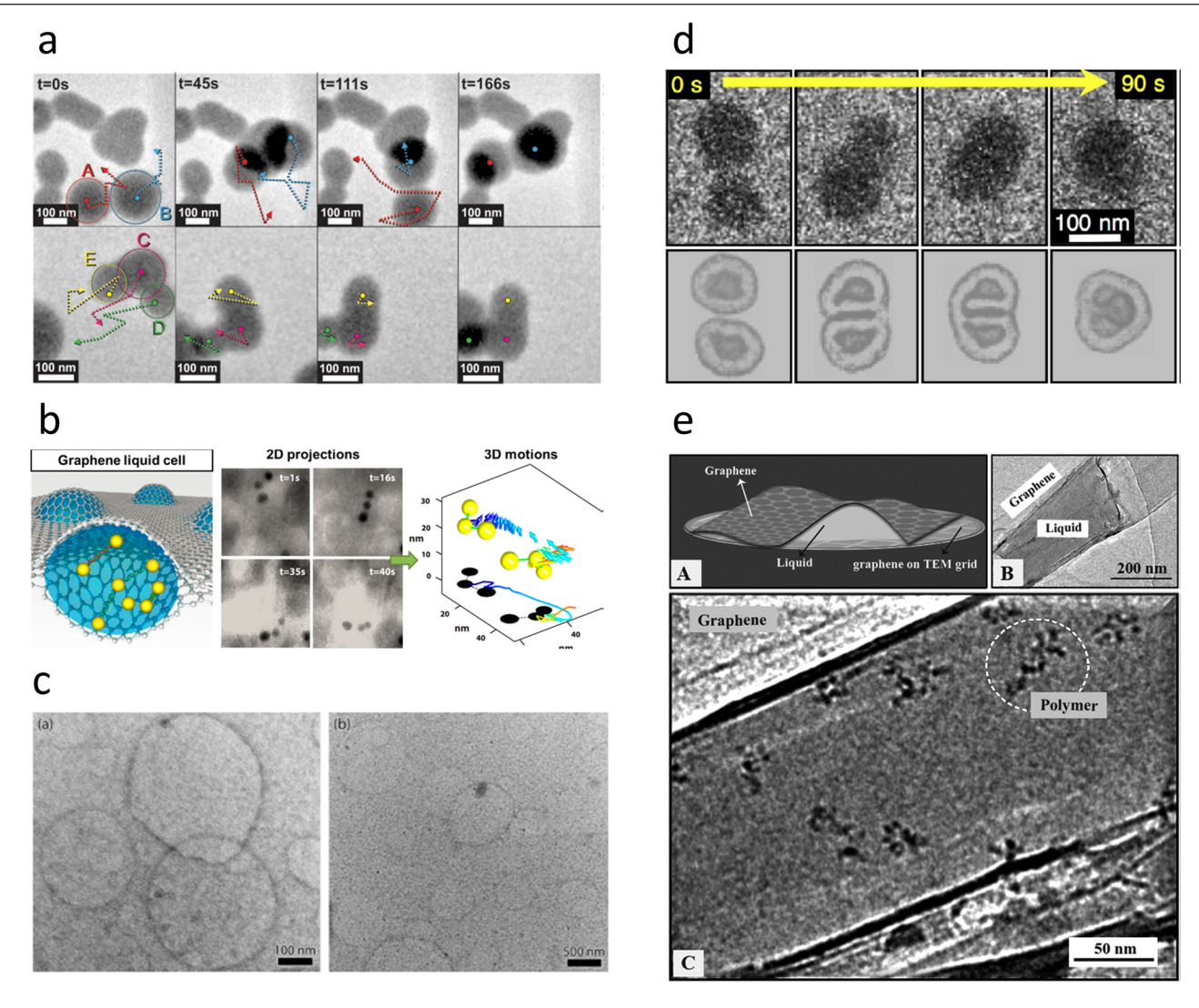


Figure 5. Liquid-cell TEM imaging of polymers and other soft molecules. (a) Time-sequential TEM images of micellar nanoparticles consisting of a Pt(II)-labeled core in water. (Reprinted with permission from [56]. Copyright 2014 American Chemical Society. (b) The 3D configuration and motion of an Au nanocrystal-ds DNA nanoconjugate trimer observed using the GLC setup. (Reprinted with permission from [57]. Copyright 2013 American Chemical Society. (c) POPC (1-palmitoyl-2-oleoyl-sn-glycero-3-phosphocholine) liposomes imaged in water. (Reprinted with permission from [76]. Copyright 2013 American Chemical Society. (d) Time-sequential images showing the micelle–micelle fusion process of amphiphilic block copolymer (BCP) micelles. (Reprinted with permission from [58]. Copyright 2017 American Chemical Society. (e) Successful imaging of individual polystyrene sulfonate (PSS) molecules using GLC [59] John Wiley & Sons. © 2017 WILEY-VCH Verlag GmbH & Co. KGaA, Weinheim.

live cells in liquid TEM by showing accumulated electrons that might kill bacteria, then it is still possible to observe live bacteria by given a short time exposure [49, 69]. The viability test of *K. pneumoniae* CG43S3 cell shows it could keep live for 50 h in sealed liquid cell, but under e-beam irritation, the time of observe live cell decrease to 100 s [70]. As a short summary, the reliability of cell imaging using liquid TEM is largely challenged by the difficulty in confirming the living status of the cell during imaging, and future work should thus focus more on how to develop reliable methods to monitor and assess the cell status.

Liquid-cell TEM method was also used to visualize the virus particles (purified rotavirus (RV) double layered particles (DLPs)) [51]. The SiN membranes were functionalized by nickel-nitrilotriacetic acid (Ni-NTA) containing lipid monolayers and adaptor proteins which limited the long-range diffusion of virus into the chips. Using this method,

different lengths of RNA strands associated with the DLPs' exterior shells were imaged as marked by the black arrows in figure 3(d). The 3D structure of the virus observed in liquid-cell was calculated and compared with the simulated 3D structure based on the cryo-TEM results. It was concluded that the structure of viruses in both techniques is perfectly matched other than 3D structure based on liquid-cell analysis with a continuum level density throughout the particles. It could be due to that the virus in liquid-cell had a higher fluidity than that of in the case of cryo-TEM [51]. It should be noted that the compositional analysis can provide detailed insights about morphological changes during liquid-cell TEM studies. To illustrate, Lewis et al [71] used the energy dispersive x-ray spectroscopy (EDS) mapping (figure 3(e)) within a liquid-cell to construct the elemental distribution of PdAu particles synthesized by a dissimilatory metal-reducing bacterium (Geobacter sulfurreducens) [50].

#### 2.2. Proteins

Apart from biological cells, proteins are more suitable to be imaged using liquid-cell TEM, because these species do not need to be alive during imaging. However, the protein has to be kept in hydrated status to achieve reliable TEM analysis. The first study using silicon nitride liquid-cells to test the protein was carried out by Evans et al [52], who reported the observation of ferritin in buffered saline solution. In this work, the iron oxide core covered by protein shell was imaged [69]. Their image line profile indicated the existence of protein shell around the iron oxide core. Macromolecules such as nanolipoprotein discs were also investigated using silicon nitride liquid-cells TEM to study the interaction between neighboring molecules [52]. The liquid TEM images were compared to negative stained and cryo-TEM images. Therefore, they concluded that the individual protein as well as complex interactions between involved macromolecular could be observed in the liquid-cell TEM. In fact, most studies reported so far have used silicon nitride liquid-cell to detect the dynamic reactions in biological samples. The biomineralization process of micelles of MamC recombinant iron-binding protein in situ by utilizing the liquid cell could be observed (figure 4(a)) [72]. But the only the initial and after stages were recorded. The bioinspired nucleation of iron oxide nanoparticles inside the negatively charged Mms6 micelle (figure 4(b)) and the nucleation process of lysozyme crystal were investigated by Kashyap et al [30] and Yamazaki et al [53], respectively. It is worth mentioning that using silicon nitride liquid cells could increase the understanding of the role of proteins in nucleation and biomineralization processes. Interestingly, the liquid iron prenucleation phase and nascent amorphous nanoparticles were found to form preferentially on the surface of protein micelles [30]. The different stages of the whole nucleation process mediated by Mms6 protein were analyzed, but the details about its dynamic were missing. In the study of lysozyme crystal formation, the assumed dense liquid was proved to be amorphous solid particles working as the heterogeneous nucleation sites, while the precursors were not able to be detected due to the resolution limitation.

Graphene sheets were also used to sandwich hydrated ferritin proteins resulting in a significantly higher spatial resolution of ~0.99 nm [54]. This was the first report on the compositional analysis of proteins inside GLC by electron energy-loss spectroscopy (EELS) (figure 4(c)). The EELS signals reflections from these proteins with and without water were also analyzed. With low dose rate imaging at 80 kV, the spatial resolution of EELS map could reach 1 nm. This work demonstrated the advantage of using graphene membranes to dramatically reduce the radiation damage of beam sensitive materials [54]. Comparing to GLC, silicon nitride liquid-cell has larger liquid volume and is easier to assembly, but GLC guarantees superior resolution that is suitable for fine spectrum analysis.

The liquid-cell TEM has also been utilized to investigate the therapeutics application of proteins. Lynn and co-workers used the microwell liquid-cell to investigate the PEGylated Interferon  $\alpha_{2a}$ , a drug-conjugate which was used to treat cancer and viral diseases [55]. The Pegasys® formulation

was proved to aggregate heat stress while acid treatment (pH  $\sim$  4.5) and freezing treatment showed only a moderate effect on the drug integrity. The aggregation of protein after heat treatment was studied in the presence/absence of contrast reagents [55]. The liquid-cell TEM could also be used to observe the membrane protein distribution and expression to test the drug reaction [33, 62–65]. Overall, using GLC to analyze protein structures could yield much higher spatial and analytical resolution in comparison to SiN-based liquid-cells.

#### 2.3. Other polymers and molecules

In addition to proteins, other polymers and molecules have also been studied by liquid-cell TEM techniques. Polymeric molecules are also typical soft materials which are composed of elements with low atomic numbers (Z < 17). In order to improve the imaging contrast, various heavy metals such as Pt(II) [56] and gold [57] have been used to label the polymeric micellar nanoparticles and DNA molecules, respectively. The motion of the polymeric micellar was dynamically tracked, and the authors implied that the driving force of the cooperative motion was beam-induced charging effect between particles (figure 5(a)) [56]. Chen et al used GLC to observe the DNA-Au nanoconjugates [57], where the dynamic trajectory of Au nanoparticles connected by double strand (dsDNA) was studied (figure 5(b)). Based on the in situ data, the 3D dynamic image of the nanoconjugate could be reconstructed. Due to minimal electron scattering from thin graphene membrane, the atomic resolution imaging of Au nanoparticles was readily achieved [57].

Liposome molecular structure at hydrated state was also investigated by liquid-cell TEM using 50 nm-thick silicon nitride membranes. The liposome was clearly observed in absence of applying any contrast enhancement methods such as staining or cryo treatment (figure 5(c)). This indicates the potential of liquid-cell TEM to image low contrast soft materials. Lucas and co-workers used a thin SiN<sub>x</sub> window (30 nm) to observe the amphiphilic micelle fusion and growth in solution [58]. In this case, the micelle was not labeled by any metal ions. In addition, the nonfusion collision and the micelle-micelle fusion and relaxation were observed and compared. The individual micelle growth by unimer attachment and insertion of solvated was also captured (figure 5(d)) [58] Later, the process of spherical micellar formation from self-assembled diblock copolymers was observed [73]. Nagamanasa et al [59] used GLC to study the conformation fluctuations of adsorbed molecules and adsorption-desorption behavior of nonmetal-ion labeled macromolecules of polystyrene sulfonate and poly(ethylene oxide). Two types of polymers were studied, namely the polystyrene sulfonate (PSS) and poly(ethylene oxide). It was reported that even at a relatively low electron dose rate (22 e  $\text{Å}^{-2}$  s<sup>-1</sup>), the polymer could only remain stable for 60 s, followed by observable degradation [59]. By controlling the dose rate and applying image reconstruction, the single polymer molecules had been captured for both two types of polymers, although no contrast differences were reported. As expected, the contrast of polymer in salt solution was weaker than that of in salt-free

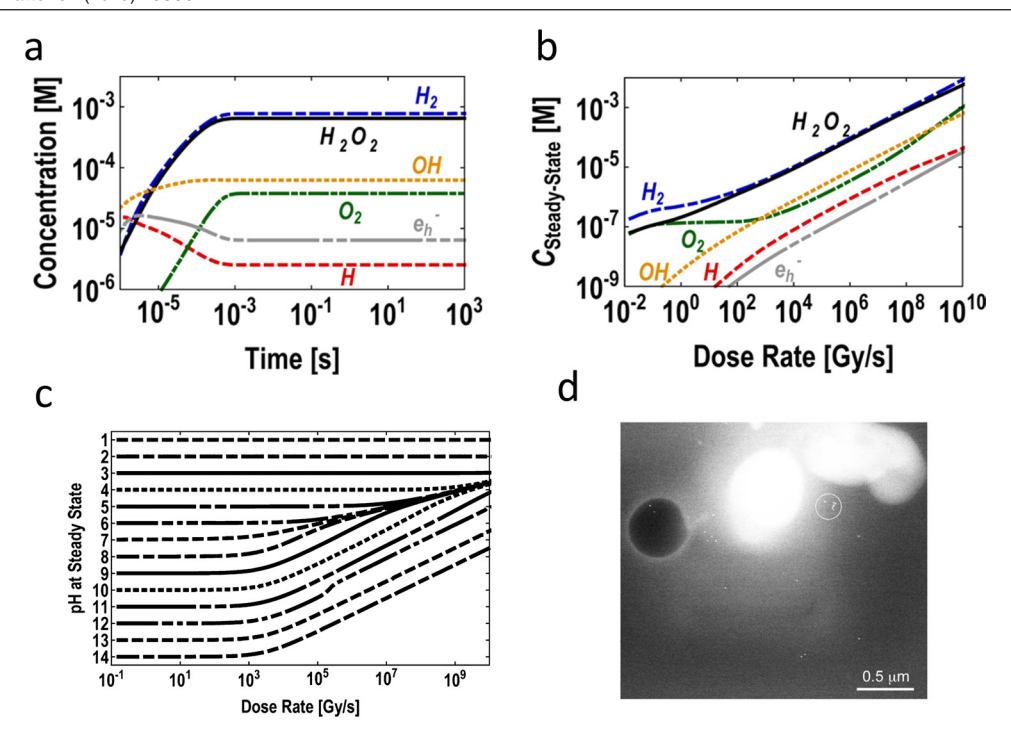


**Figure 6.** Electron beam effect during imaging of liquid solutions. (a) Concentrations of  $e_{aq}^-$ ,  $H^{\bullet}$ ,  $H_2$ ,  $H_2O_2$ ,  $OH^{\bullet}$ , and  $O_2$  as function of beam exposure time of the solution. (b) Steady state concentration of  $e_{aq}^-$ ,  $H^{\bullet}$ ,  $H_2$ ,  $H_2O_2$ ,  $OH^{\bullet}$ , and  $O_2$  species as a function of dose rate. (c) The steady state of pH as a function of dose rate. Reprinted with permission from [78]. Copyright 2014 American Chemical Society. (d) Typical beam damages such as hole generation and contamination occurred during the imaging. Reproduced from [23]. CC BY 4.0.

solution. However, the diffusion of polymer was more sluggish than it was in salt-free solution. The reason was ascribed to the adsorption from graphene caused by, hydrophobic interactions [74], or chemisorption [59]. Besides the electron beam-induced polymerization, the electrochemical deposition of poly(3,4-ethylenedioxythiophene) (PEDOT) could also be investigated using electrochemical liquid-cell TEM [75]. The deposition of PEDOT was first detected at the edge of the working electrode, following by the liquid-like oligomers close to the electrode [75]. Generally, liquid-cell TEM using GLC provides higher spatial resolution but the motion of targeted materials might be affected more by the adsorption from adjacent graphene layers. Imaging using silicon nitride liquid-cell has less side effects on the monitoring of material motion, while this is at the expense of the spatial resolution.

#### 2.4. Radiolysis and beam effect during liquid-cell imaging

The main concern of the liquid-cell TEM imaging is the effect of electron beam on the targeted materials and the alteration of chemical environment surrounding of the materials. Soft materials, in particular biological cells, bacteria and proteins, are much more sensitive to the electron beam than inorganic or hard materials. The radiation pressures of accelerated electron beam can cause shear force on soft materials. But the radiation pressure caused force is proved to falling into femtonewton range [77], which is relative small for the soft materials especially the biological cell. The liquid surrounding samples also decrease the shear force caused by the radiation pressure. For most of the soft materials, aqueous media is used to preserve the structure of interests. It is thus critical to know the radiolysis products of water when exposed to electron beam, and the

effect of electron beam on the soft materials in the aqueous solution. Water can be decomposed into several species when irradiated by electron beam: hydrated electrons  $e_{aq}^-$ , hydrogen radical H $^{\bullet}$ , hydroxyl OH $^{\bullet}$ , hydrogen H $_2$ , hydrogen peroxide H $_2$ O $_2$ , hydron H $^+$ , oxygen O $_2$ , and hydroxide OH $^-$  [78–80]. These radicals change the chemical or pH of the solution, which may subsequently trigger unexpected reactions. To understand such effects, the electron dose influencing the solution needs to be quantified. There are two ways to calculate the dose rate. One way is Gy s $^{-1}$ , using function:

$$\Psi = \frac{S \cdot 10^5 I}{A}.\tag{1}$$

For this function,  $\Psi$  is the dose rate for a thin liquid layer. The parameter S (Mev cm<sup>2</sup> g<sup>-1</sup> electron) is the density-normalized stopping power in the medium; I is the illumination current (e<sup>-</sup> s<sup>-1</sup>), and A (Å<sup>2</sup>) is the illuminated area [78, 79]. By this function, the absorption energy of the irradiated medium could be calculated. But the generally used dose rate is calculated based on the equation:

$$D_{\rm r} = I/eA \tag{2}$$

where  $D_r$  is electron dose rate (e/Ų/s); I is the beam current; e is the elementary charge (C/electron) and A is the scanning area (Ų). Schneider et al [78] calculated the interaction of these species with incident electrons. Based on their results (figure 6(a)), the concentrations of  $e_{aq}^-$ ,  $H^{\bullet}$ ,  $H_2$ ,  $H_2O_2$ ,  $OH^{\bullet}$ , and  $O_2$  species are a function of time. In a constant dose rate, the concentrations of all these species, (in initially neat deaerated water), reach steady state values within the same time frame. The calculation of different dose also demonstrates that the eventual establishment of the steady state is related to the

dose rate (figure 6(b)). The pH of the solution, which could be altered by the concentration of H<sup>+</sup>, is also changed by the e-beam irradiation. The steady state of pH is relied on dose rate and the initial pH of deaerated water, as shown in figure 6(c). In a lower dose rate ( $<10^3$  Gy s<sup>-1</sup> or  $<\sim10^{-4}$  e/Å<sup>2</sup>/s), the pH of the solution is almost the same as the initial value. For higher dose rates, the pH is affected by the dose rate and the initial pH value. For solutions with an initial pH > 3, the pH can approach to 3 with an increase in dose rate. It indicates that the e-beam has a strong effect on alkaline solutions [78]. However, cases are different when the solutions are changed to other types such as methanol and acetone, where the redox species generated by e-beam are different from that of in the aqueous solution.

Overall, it is expected that the local chemical environment affected by electron beam can be minimized by the flow of liquid rather than keeping the liquid in static state. By taking the advantage of the energy delivered via the incident electrons, liquid-cells can be intentionally used as a nanoreactor for reactions such as nucleation/growth and etching/dissolution. The behaviors of Au nanoparticles under different pHs and various concentrations of sodium chloride were studied using *in situ* liquid-cell TEM [13]. The etching/dissolution process in the liquid-cell is ascribed to high-energy electrons [78, 81–86].

Besides the radicals generated by e-beam, the energy transferred from the incident electrons to the soft materials needs to be considered. The lowest threshold energies for carbon and phosphor displacements are 25 eV and 10 eV, respectively [87]. This means that at a voltage over 25 V, these atoms could possibly be knocked out by the incident electrons. What's worse, since cells and bacteria generally have large volume, the incident electrons have to travel a longer distance before they can escape from the sample, which thus results in more inelastic scattering. Figure 6(d) shows two types of beam damages on liquid-cell TEM, where a black hole was generated by e-beam, and a whitish area was appeared by contamination.

Another important aspect of live cell imaging is the threshold lethal dose below which the biological structure could be imaged safely. The lethal dose is reported to be  $29.4~\rm e^-~nm^{-2}$  for killing 50% of *E. coli* bacteria in liquid-cell TEM under  $300\,\rm kV$  [49]. For whole fixed COS7 fibroblasts, the cells can be kept undamaged at  $10~\rm e^-~\mathring{A}^{-2}$  to  $10^3~\rm e^-~\mathring{A}^{-2}$  under  $30\,\rm kV$  [88]. The lethal dose for *E. coli* is 50 kilorads for pulsed e-beam under  $520\,\rm kV$  [89]. Therefore, it is apparent that the suitable dose depends not only on the properties of the specimens, but also on the choice of solutions as well as the control of the e-beam conditions.

#### 3. Outlook

Here, we reviewed the application of liquid TEM technique in the study of soft materials such as biological cells, bacteria, viruses, proteins and macromolecules. All these soft materials are made of low atomic number elements. In spite of the recent development in TEM imaging of such materials, it should be also realized that the existence of a significant advance to improve the current state of TEM imaging to obtain more reliable information about the dynamics of soft materials and biological structures is crucial. Rooted in the current fundamentals enabled by liquid TEM as reviewed here, we thus propose the following directions as future research perspectives that are highly desired and also holding a promise to be achieved given the advent of breakthroughs in either material design or device development.

#### 3.1. Elemental analysis in liquid cells

For most TEM studies of soft materials, the composition analysis is generally carried out after the in situ liquid experiments or through cryo TEM. Therefore, it is desirable to spend more effort on the enhancement of the nanoscale analytical capability during in situ TEM experiments using techniques such as EDS [50] and EELS [54]. One importance parameter is the balance of the spatial and analytical resolutions with the amount of liquid enclosed in the liquid cells. GLCs can give higher spatial resolution, but the liquid pocket of GLC is just around 100-300 nm [90]. To encapsulate more liquid, the monolayer graphene should be large enough to sandwich the cell/bacteria and preserve enough liquid in interlayer space of the graphene sheets. One option is to use another 2D materials to replace graphene. This 2D material should be rigid enough to survive in high vacuum environment such as microscope column, and also need to be impermeable to the trapped liquids.

#### 3.2. Effect of internal pressure of liquid cells

In graphene liquid cells, due to van der Waals interactions between graphene sheets, it is anticipated that a high internal pressure might be exerted on the materials encapsulated in interlayer space of graphene sheets. The van der Waals pressure between two graphene layers could be estimated based on equation  $P \approx E/d$ , where E is the adhesion energy and d is a typical interlayer distance [91]. For liquid/graphene interface, the thinner the cell is, the higher the pressure will be. Based on above mentioned equation, the pressure generated by two graphene layers in a 300 nm-spaced GLC can be higher than 1 MPa. Another way to calculate the pressure between two graphene layers is based on equation  $\Delta P = 2\gamma/R_c$ , where  $\Delta P$ is the pressure difference across the liquid/graphene interface,  $\gamma$  is the surface tension of water and  $R_c$  is the radius of curvature in GLC [92]. According to this equation, the pressure of a 300 nm-spaced GLC could be around 0.9 MPa. This pressure is about ten times greater than atmosphere pressure. Therefore, the pressure inside a GLC can be controlled by the spacing between graphene sheets and the amount of liquids trapped in between.

#### 3.3. Taking advantage of the nanoscale confinement

While there might be certain side effect from the nanoscale confinement geometry during liquid cell imaging [45, 73, 93], it could also be a revolutionary advancement if such confinement

can be utilized to mimic the biological environment for certain reactions that are originally in similar nanoscale confinement condition. Exampled reactions include, but are not limited to, the nucleation process of ferritin in protein cage [94] and the mineralization process of hydroxyapatite in collagen [95]. For these processes, the graphene or SiN membrane could be further functionalized by protein or molecules, which, combining with the simulation solution, can be potentially applied as a nano reactor that maximizes the similarity between liquid cell imaging operation and the real biological conditions.

#### 3.4. Enabling fluidic mixing in GLCs

Although the GLC provides high imaging resolution with the spectroscopic capability, it only allows static mode observation and only one liquid can be enclosed at one time. It will be impressing if we could provide condition to flow the solution mixing in GLCs by manipulating the electron beam to generate bubbles and create bridge between two or more GLC pockets for solution mixing. This could result in effective observation of solution reaction dynamics with analytical capability and at high spatial resolution.

#### 3.5. Studies of living organisms

There are some reports about using the liquid cells to observe the nanoparticles formed inside bacteria (i.e. magnetotactic bacteria) such as iron oxide nanoparticles [46]. However, the dynamic formation process of these nanoparticles inside the bacteria and their evolution pathways inside live bacteria are currently unclear. With the development of the liquid-cell technique, various stimuli such as bias and heat are expected to be introduced into the liquid environment to provoke the nanoscale response of organisms [96]. The pH of the solution can be also changed with the dose rate [78]. The pH dependent reactions could be studied by controlling the dose rate and initial pH. It should be also noted that during TEM imaging, the electron beam can generate various radiolysis products [78]. Therefore, attention should be given to control the dose rate and carefully evaluate the effect of radiolysis products on the living organisms.

#### **Acknowledgments**

R Shahbazian-Yassar acknowledges the financial support from the National Science Foundation (NSF) Division of Materials Research (DMR) Award No. 1710049. T Shokuhfar's efforts are supported by NSF-CBET Award No. 1803693.

#### **ORCID iDs**

Kun He https://orcid.org/0000-0001-5504-5458
Tolou Shokuhfar https://orcid.org/0000-0002-7905-2748
Reza Shahbazian-Yassar https://orcid.org/0000-0002-7744-4780

#### References

- [1] Bartesaghi A, Merk A, Banerjee S, Matthies D, Wu X, Milne J L and Subramaniam S 2015 *Science* **348** 1147–51
- [2] Zhang X, Jin L, Fang Q, Hui W H and Zhou Z H 2010 Cell 141 472–82
- [3] Li X, Mooney P, Zheng S, Booth C R, Braunfeld M B, Gubbens S, Agard D A and Cheng Y 2013 Nat. Methods 10 584
- [4] Liao M, Cao E, Julius D and Cheng Y 2013 Nature 504 107
- [5] Murphy G E, Narayan K, Lowekamp B C, Hartnell L M, Heymann J A, Fu J and Subramaniam S 2011 J. Struct. Biol. 176 268–78
- [6] Brubacher J L, Vieira A P and Newmark P A 2014 Nat. Protocols 9 661
- [7] Thompson R F, Walker M, Siebert C A, Muench S P and Ranson N A 2016 Methods 100 3–15
- [8] Ohi M, Li Y, Cheng Y and Walz T 2004 Biol. Proc. 6 23
- [9] Evans J E 2007 Visualizing Biology from Atoms to Cells (Davis, CA: University of California)
- [10] De Carlo S and Stark H 2010 Cryonegative staining of macromolecular assemblies *Methods Enzymol.* 481 127–45
- [11] Dubochet J, Adrian M, Chang J-J, Homo J-C, Lepault J, Mcdowall A W and Schultz P 1988 Q. Rev. Biophys. 21 129–228
- [12] Kraus T and De Jonge N 2013 Langmuir 29 8427–32
- [13] Áde Jonge N 2015 Chem. Commun. 51 16393-6
- [14] Song B, He K, Yuan Y, Sharifi-Asl S, Cheng M, Lu J, Saidi W A and Shahbazian Yassar R 2018 Nanoscale 10 15809–18
- [15] Evans J E, Jungjohann K L, Browning N D and Arslan I 2011 Nano Lett. 11 2809–13
- [16] Liao H G, Niu K and Zheng H 2013 Chem. Commun. 49 11720–7
- [17] Wu F and Yao N 2015 Nano Energy 11 196-210
- [18] Zeng Z, Liang W-I, Chu Y H and Zheng H 2014 Faraday Discuss. 176 95–107
- [19] Cheong J Y, Chang J H, Seo H K, Yuk J M, Shin J W, Lee J Y and Kim I-D 2016 Nano Energy 25 154–60
- [20] Gu M et al 2013 Nano Lett. 13 6106-12
- [21] Holtz M E, Yu Y, Gunceler D, Gao J, Sundararaman R, Schwarz K A, Arias T A, Abruna H D and Muller D A 2014 Nano Lett. 14 1453–9
- [22] He K, Bi X, Yuan Y, Foroozan T, Song B, Amine K, Lu J and Shahbazian-Yassar R 2018 Nano Energy 49 338–45
- [23] Peckys D B, Veith G M, Joy D C and De Jonge N 2009 PLoS One 4 e8214
- [24] Williamson M J, Tromp R M, Vereecken P M, Hull R and Ross F M 2003 *Nat. Mater.* **2** 532–6
- [25] Lutz L, Dachraoui W, Demortière A, Johnson L R, Bruce P G, Grimaud A and Tarascon J-M 2018 Nano Lett. 18 1280–9
- [26] Piffoux M, Ahmad N, Nelayah J, Wilhelm C, Silva A, Gazeau F and Alloyeau D 2018 Nanoscale 10 1234–44
- [27] Nielsen M H, Aloni S and De Yoreo J J 2014 Science 345 1158–62
- [28] Abellan P, Mehdi B L, Parent L R, Gu M, Park C, Xu W, Zhang Y, Arslan I, Zhang J-G and Wang C-M 2014 Nano Lett. 14 1293–9
- [29] Sacci R L, Dudney N J, More K L, Parent L R, Arslan I, Browning N D and Unocic R R 2014 Chem. Commun. 50 2104–7
- [30] Kashyap S, Woehl T J, Liu X, Mallapragada S K and Prozorov T 2014 ACS Nano 8 9097–106
- [31] Hermannsdörfer J and De Jonge N 2017 *J. Vis. Exp.* **120** 54943
- [32] Zheng H, Smith R K, Jun Y-W, Kisielowski C, Dahmen U and Alivisatos A P 2009 Science 324 1309–12

- [33] Dahmke I N, Verch A, HermannsdöRfer J, Peckys D B, Weatherup R S, Hofmann S and De Jonge N 2017 ACS Nano 11 11108–17
- [34] Textor M and De Jonge N 2018 Nano Lett. 18 3313-21
- [35] Frank I, Tanenbaum D M, Van Der Zande A M and Mceuen P L 2007 J. Vac. Sci. Technol. B 25 2558–61
- [36] Mohanty N, Fahrenholtz M, Nagaraja A, Boyle D and Berry V 2011 Nano Lett. 11 1270–5
- [37] Wang X, Zhi L and Müllen K 2008 Nano Lett. 8 323-7
- [38] Kim K S, Zhao Y, Jang H, Lee S Y, Kim J M, Kim K S, Ahn J-H, Kim P, Choi J-Y and Hong B H 2009 *Nature* **457** 706
- [39] Huang Y, Wu J and Hwang K-C 2006 *Phys. Rev.* B **74** 245413
- [40] Nemes-Incze P, Osváth Z, Kamarás K and Biró L 2008 Carbon 46 1435–42
- [41] Yuk J M, Park J, Ercius P, Kim K, Hellebusch D J, Crommie M F, Lee J Y, Zettl A and Alivisatos A P 2012 Science 336 61–4
- [42] De Jonge N, Peckys D B, Kremers G and Piston D 2009 Proc. Natl Acad. Sci. 106 2159–64
- [43] Pohlmann E S, Patel K, Guo S, Dukes M J, Sheng Z and Kelly D F 2015 *Nano Lett.* **15** 2329–35
- [44] Peckys D B, Baudoin J-P, Eder M, Werner U and De Jonge N 2013 Sci. Rep. 3 2626
- [45] Moser T H, Mehta H, Park C, Kelly R T, Shokuhfar T and Evans J E 2018 *Sci. Adv.* 4 eaaq1202
- [46] Woehl T J, Kashyap S, Firlar E, Perez-Gonzalez T, Faivre D, Trubitsyn D, Bazylinski D A and Prozorov T 2014 Sci. Rep. 4 6854
- [47] Prozorov T, Almeida T P, Kovács A and Dunin-Borkowski R E 2017 J. R. Soc. Interface 14 20170464
- [48] Kennedy E, Nelson E M, Tanaka T, Damiano J and Timp G 2016 ACS Nano 10 2669–77
- [49] Kennedy E, Nelson E M, Damiano J and Timp G 2017 ACS Nano 11 3–7
- [50] Lewis E A, Downie H, Collins R F, Prestat E, Lloyd J R and Haigh S J 2016 *Part. Part. Syst. Charact.* **33** 833–41
- [51] Varano A C, Rahimi A, Dukes M J, Poelzing S, Mcdonald S M and Kelly D F 2015 Chem. Commun. 51 16176–9
- [52] Evans J E, Jungjohann K L, Wong P C, Chiu P L, Dutrow G H, Arslan I and Browning N D 2012 Micron 43 1085–90
- [53] Yamazaki T, Kimura Y, Vekilov P G, Furukawa E, Shirai M, Matsumoto H, Van Driessche A E and Tsukamoto K 2017 Proc. Natl Acad. Sci. 114 2154–9
- [54] Wang C, Qiao Q, Shokuhfar T and Klie R F 2014 Adv. Mater. 26 3410–4
- [55] Dimemmo L M, Varano A C, Haulenbeek J, Liang Y, Patel K, Dukes M J, Zheng S, Hubert M, Piccoli S P and Kelly D F 2017 Lab Chip 17 315–22
- [56] Proetto M T et al 2014 J. Am. Chem. Soc. 136 1162-5
- [57] Chen Q, Smith J M, Park J, Kim K, Ho D, Rasool H I, Zettl A and Alivisatos A P 2013 Nano Lett. 13 4556–61
- [58] Parent L R, Bakalis E, Ramírez-Hernández A, Kammeyer J K, Park C, De Pablo J, Zerbetto F, Patterson J P and Gianneschi N C 2017 J. Am. Chem. Soc. 139 17140–51
- [59] Nagamanasa K H, Wang H and Granick S 2017 Adv. Mater. 29 1703555
- [60] Klein K, Anderson I and De Jonge N 2011 J. Microsc. 242 117–23
- [61] Reifarth M, Hoeppener S and Schubert U S 2018 Adv. Mater. 30 1703704
- [62] Peckys D B, Stoerger C, Latta L, Wissenbach U, Flockerzi V and De Jonge N 2017 J. Struct. Biol. 199 102–13
- [63] Peckys D B, Korf U and De Jonge N 2015 Sci. Adv. 1 e1500165
- [64] De Jonge N 2018 J. Microsc. 269 134-42
- [65] Peckys D B, Korf U, Wiemann S and De Jonge N 2017 Mol. Biol. Cell 28 3193–202

- [66] Wang Y, Chen X, Cao H, Deng C, Cao X and Wang P 2015 J. Anal. Methods Chem. 2015 269–76
- [67] De Jonge N and Peckys D B 2016 ACS Nano 10 9061-3
- [68] Peckys D B, Mazur P, Gould K L and De Jonge N 2011 Biophys. J. 100 2522–9
- [69] Evans J E and Browning N D 2013 Microscopy 62 147–56
- [70] Liu K-L, Wu C-C, Huang Y-J, Peng H-L, Chang H-Y, Chang P, Hsu L and Yew T-R 2008 Lab Chip 8 1915–21
- [71] Lewis E A, Haigh S J, Slater T J, He Z, Kulzick M A, Burke M G and Zaluzec N J 2014 Chem. Commun. 50 10019–22
- [72] Kashyap S, Woehl T, Valverde-Tercedor C, Sánchez-Quesada M, López C J and Prozorov T 2014 J. Nanomater. 2014 1
- [73] Touve M A, Figg C A, Wright D B, Park C, Cantlon J, Sumerlin B S and Gianneschi N C 2018 ACS Central Sci. 4 543–7
- [74] Georgakilas V, Otyepka M, Bourlinos A B, Chandra V, Kim N, Kemp K C, Hobza P, Zboril R and Kim K S 2012 Chem. Rev. 112 6156–214
- [75] Liu J, Wei B, Sloppy J D, Ouyang L, Ni C and Martin D C 2015 ACS Macro Lett. 4 897–900
- [76] Hoppe S M, Sasaki D Y, Kinghorn A N and Hattar K 2013 Langmuir 29 9958–61
- [77] Pairis S, Donatini F, Hocevar M, Tumanov D, Vaish N, Claudon J, Poizat J-P and Verlot P 2018 (arXiv:1803.09312)
- [78] Schneider N M, Norton M M, Mendel B J, Grogan J M, Ross F M and Bau H H 2014 J. Phys. Chem. C 118 22373–82
- [79] Wang C, Shokuhfar T and Klie R F 2016 Adv. Mater. 28 7716–22
- [80] Abellan P, Woehl T J, Parent L R, Browning N D, Evans J E and Arslan I 2014 Chem. Commun. 50 4873–80
- [81] Yuan Y, Wood S M, He K, Yao W, Tompsett D, Lu J, Nie A, Islam M S and Shahbazian-Yassar R 2016 ACS Nano 10 539–48
- [82] Park J H, Schneider N M, Grogan J M, Reuter M C, Bau H H, Kodambaka S and Ross F M 2015 Nano Lett. 15 5314–20
- [83] Ngo T and Yang H 2015 J. Phys. Chem. Lett. 6 5051-61
- [84] Chee S W, Pratt S H, Hattar K, Duquette D, Ross F M and Hull R 2014 *Chem. Commun.* 51 168–71
- [85] Jiang Y, Zhu G, Dong G, Lin F, Zhang H, Yuan J, Zhang Z and Jin C 2017 Micron 97 22–8
- [86] Patterson J P, Abellan P, Denny M S Jr, Park C, Browning N D, Cohen S M, Evans J E and Gianneschi N C 2015 J. Am. Chem. Soc. 137 7322–8
- [87] Konobeyev A Y, Fischer U, Korovin Y A and Simakov S 2017 Nucl. Energy Technol. 3 169–75
- [88] Hermannsdörfer J, Tinnemann V, Peckys D B and De Jonge N 2016 Microsc. Microanal. 22 656–65
- [89] Epp E R, Weiss H and Santomasso A 1968 *Radiat. Res.* **34** 320–5
- [90] Sasaki Y, Kitaura R, Yuk J M, Zettl A and Shinohara H 2016 Chem. Phys. Lett. 650 107–12
- [91] Algara-Siller G, Lehtinen O, Wang F, Nair R, Kaiser U, Wu H, Geim A and Grigorieva I 2015 Nature 519 443
- [92] Shin D, Park J B, Kim Y-J, Kim S J, Kang J H, Lee B, Cho S-P, Hong B H and Novoselov K S 2015 Nat. Commun. 6 6068
- [93] Kröger R and Verch A 2018 Minerals 8 21
- [94] Narayanan S, Firlar E, Shafiee S, He K, Shahbazian-Yassar R and Shokuhfar T 2017 Microsc. Microanal. 23 1184–5
- [95] Nudelman F, Pieterse K, George A, Bomans P H, Friedrich H, Brylka L J, Hilbers P A, De With G and Sommerdijk N A 2010 Nat. Mater. 9 1004
- [96] Jack J J B, Noble D and Tsien R W 1975 *Electric Current Flow in Excitable Cells* (Oxford: Clarendon Press) p 5